

# From Bioreactor to Bulk Rheology: Achieving Scalable Production of Highly Concentrated Circular DNA

Wynter A. Paiva, Somkene D. Alakwe, Juexin Marfai, Madigan V. Jennison-Henderson, Rachel A. Achong, Tinotenda Duche, April A. Weeks, Rae M. Robertson-Anderson, and Nathan J. Oldenhuis\*

DNA serves as a model system in polymer physics due to its ability to be obtained as a uniform polymer with controllable topology and nonequilibrium behavior. Currently, a major obstacle in the widespread adoption of DNA is obtaining it on a scale and cost basis that accommodates bulk rheology and high-throughput screening. To address this, recent advancements in bioreactor-based plasmid DNA production is coupled with anion exchange chromatography producing a unified approach to generating gram-scale quantities of monodisperse DNA. With this method, 1.1 grams of DNA is obtained per batch to generate solutions with concentrations up to 116 mg mL<sup>-1</sup>. This solution of uniform supercoiled and relaxed circular plasmid DNA, is roughly 69 times greater than the overlap concentration. The utility of this method is demonstrated by performing bulk rheology measurements at sample volumes up to 1 mL on DNA of different lengths, topologies, and concentrations. The measured elastic moduli are orders of magnitude larger than those previously reported for DNA and allowed for the construction of a time-concentration superposition curve that spans 12 decades of frequency. Ultimately, these results can provide important insights into the dynamics of ring polymers and the nature of highly condensed DNA dynamics.

## 1. Introduction

In materials science and biotechnology, DNA transcends its conventional biological role where it is often used as a sequence defined polymer with programmable structural and functional elements. Indeed, recent decades have witnessed an explosion of DNA-based approaches to directed self-assembly of bespoke materials.<sup>[1–7]</sup> DNA has also been employed as a model system to address fundamental questions in polymer physics, ranging from the dynamics of single polymers to rheological properties of highly entangled solutions.<sup>[8–12]</sup>

One key advantage of DNA over synthetic polymers lies in the ability to prepare uniform samples, i.e., polymers with precisely the same length. In contrast, methods used to prepare synthetic polymers typically result in a dispersity index above 1.<sup>[9,11,13–18]</sup> DNA also forms entanglements at very low volume fractions (<1%) compared to synthetic polymers which typically require much higher concentrations. This enables the testing of predicted concentration scaling of rheological properties

and tuning of polymer properties through modulation of buffer conditions.<sup>[9,10,13,19–23]</sup> Furthermore, plasmid DNA (pDNA) can easily be isolated from bacteria and occurs in a unique natively supercoiled circular (SC) topology. Common commercially available enzymes can then be used to relax SC DNA into the relaxed open circular (OC/ring) isoform or cut open to produce the linear (L) isoform. These enzymes operate with a high degree of selectivity and exceptional accuracy for predictable generation of three distinct polymers that only differ in topology.<sup>[13,15,18,20,24]</sup>

This robust control over topology and ability to form entanglements has been leveraged to shed light on the highly debated dynamics of ring polymers.<sup>[13,16,17,19,20,25,26–33]</sup> Entangled linear polymers can be described by the celebrated reptation model which treats each polymer as being confined to a tube-like region formed by the surrounding polymers.<sup>[13]</sup> This restricts the chain's lateral motion, and forces diffusion to proceed “head-first” along the contour of the tube.<sup>[13]</sup> Conversely, ring polymers cannot undergo traditional reptation as these models depend upon the behavior that arises from free ends

W. A. Paiva, S. D. Alakwe, M. V. Jennison-Henderson, R. A. Achong, T. Duche, A. A. Weeks, N. J. Oldenhuis  
 Department of Chemistry, College of Engineering and Physical Science  
 University of New Hampshire  
 23 Academic Way, Parsons Hall, Durham NH 03824, USA  
 E-mail: [nathan.oldenhuis@usnh.edu](mailto:nathan.oldenhuis@usnh.edu)

J. Marfai, R. M. Robertson-Anderson  
 Department of Physics and Biophysics  
 College of Arts and Sciences  
 University of San Diego  
 Shiley Center for Science and Technology  
 5998 Alcalá Park, San Diego, CA 92110, USA

 The ORCID identification number(s) for the author(s) of this article can be found under <https://doi.org/10.1002/adma.202405490>

© 2024 The Author(s). Advanced Materials published by Wiley-VCH GmbH. This is an open access article under the terms of the [Creative Commons Attribution-NonCommercial-NoDerivs](https://creativecommons.org/licenses/by/4.0/) License, which permits use and distribution in any medium, provided the original work is properly cited, the use is non-commercial and no modifications or adaptations are made.

DOI: 10.1002/adma.202405490

which are not present in rings. Due to this key difference in topology, the extent to which cyclic polymers form entanglements and undergo “modified reptation” is a topic of extreme debate.<sup>[13,16,17,19,20,25,26–33]</sup> Further, the rheological properties of supercoiled polymers are even less understood, despite the relevance to DNA in the nucleus, and similarities to branched polymers. The challenge of studying ring polymers dynamics is exacerbated by the presence of linear contaminants, which can substantially modify the mechanical properties even in trace amounts.<sup>[13,16–20,25,31,34]</sup> These linear contaminants are ubiquitous in synthetic ring polymers due to the cyclization processes used to make them causing scientists to seek alternative sources.<sup>[13,17]</sup> Even large pDNA samples (> 25 kbp) are susceptible to shear induced linearization complicating their use.<sup>[13,18,35]</sup> Consequently, the inability to access uniform samples of highly pure ring polymers remains a major challenge in the development of accurate models to describe their dynamics.

Compounding this challenge is the need to from solutions of ring polymers well above the critical entanglement concentration at quantities amenable to bulk rheology.<sup>[13,15,18,25]</sup> This lack of scalability is indeed a problem across all DNA materials, as DNA-based self-assembly also requires large quantities of DNA with well-defined topology and controllable sequences.<sup>[1–7]</sup> Unfortunately, current methods for large-scale fermentation and purification fall short of meeting this demand and produce  $\approx 1$ – $10$  mg of DNA per batch at concentrations of  $\leq 10$  mg mL<sup>-1</sup>.<sup>[15]</sup> The low entanglement density in these solutions require volumes of  $\approx 300$ – $500$   $\mu$ L for sufficiently sensitive bulk rheology measurements, permitting only  $\approx 3$  measurements per batch. Further complicating these methods, isolation of DNA from bacterial cells requires removal of cellular RNA, typically done by RNase treatment or additional chromatographic steps which are costly and time consuming at larger scales.<sup>[36–39]</sup>

To address this challenge, we present a new method for producing gram-scale quantities of purified pDNA at concentrations nearly three orders of magnitude above the coil overlap concentration,  $c^*$  ( $\approx 10^2$  mg mL<sup>-1</sup>,  $\approx 69$   $c^*$ ). At a rough cost of \$1.4 per mg of DNA, this method represents a two orders of magnitude increase in yield and  $\approx 2$ -fold decrease in cost over current bulk purification methods (\$2.7 per mg DNA) and  $\approx 100$  fold decrease over commercial sources (\$100–1000 per mg DNA).<sup>[15]</sup> We accomplish this by leveraging advancements in nucleic acid vaccine manufacturing to serve as a starting point for accessing gram-scale quantities of DNA for use in academic research. Specifically, in the past 20 years, there has been a notable surge in the utilization of bioreactor-based techniques to produce pDNA.<sup>[40]</sup> This approach proved crucial in the response to the COVID-19 pandemic, vital for in vitro transcribed mRNA production.<sup>[41]</sup> Bioreactors achieve high optical densities ( $OD_{600} > 100$ ) by extending the bacterial exponential growth phase through inline monitoring, active feeding, and increased aeration. Continuous optimization has increased pDNA yields up to  $2.6$  g L<sup>-1</sup> corresponding to a roughly  $10^3$ -fold improvement over conventional methods.<sup>[42–47]</sup> To accommodate this increased scale, lysis and purification strategies utilizing anion exchange chromatography (AEX) were developed to minimize costs and enhance throughput.<sup>[36–39,48]</sup> These processes are employed on the  $> 10^4$  L scale to obtain kilograms of pDNA for direct vaccination or mRNA transcription.

As these methods have gained popularity, the costs of “benchtop” bioreactors and AEX resins have continued to decrease making them practical to obtain in academic research labs. Unfortunately, many industrial processes are reported as single bioprocess steps that are not published in detail to the public.<sup>[44]</sup> Furthermore, most of these methods utilize costly or industry specific apparatuses not commonly available in an academic setting. Therefore, we sought the development of a unified method that harnesses the advancements in DNA production and purification while employing resources readily available to academic laboratories with the end goal of studying highly concentrated solutions of monodisperse DNA of varying topologies (Figure 1). Here, we demonstrate the power of this approach by purifying pDNA constructs of  $\approx 3$ – $45$  kbp, which we chose to maximize the yield of SC topologies and prevent inadvertent linearization of circular constructs.

## 2. Results and Discussion

Here, we describe the various steps in our bioprocess (Figure 1), the important considerations to maximize yield and reproducibility, and our results demonstrating their effectiveness. Full detailed protocols are provided in the Experimental Section. Following the steps outlined in Figure 1, which include fermentation, isolation, and purification, we demonstrate successful preparation of five plasmids: pUC19 (2.686 kbp), pUCBB-pT7-eGFP (pEGFP, 3.075 kbp), pUCP20T-eYFP (pEYFP, 5.045 kbp), pPIC11 (11 kbp), and Fos45 (45 kbp) (Figure 2). Analysis for the purification of pEYFP is reported below while all others are reported in Figures S1–S4 (Supporting Information). We achieve yields up to  $208$  mg L<sup>-1</sup> weight plasmid per liter of culture fluid and final solution concentrations up to  $116$  mg mL<sup>-1</sup>. We chose pPIC11 and Fos45 as two of our targets to directly compare our yields to those from previously reported methods.<sup>[15]</sup> Using our approach, we achieve orders of magnitude increase in yield of pPIC11 and Fos45 to  $83$  and  $125$  mg L<sup>-1</sup> respectively. This allowed us to generate a stock solution of pPIC11 with a concentration of  $116$  mg mL<sup>-1</sup>.

### 2.1. Fermentation

The first step in the process is cell growth which requires precise calibration and maintenance of monitoring probes. We found that inaccurate monitoring or control over the culture environment led to significantly lower yields, even when high biomass accumulation was observed. Early in the fermentation process, cell growth was limited and did not significantly impact the optical density ( $OD_{600}$ ), pH or dissolved oxygen (DO) of the culture media. After  $\approx 5$  h, cell growth became evident from the increased  $OD_{600}$  (Figure 3A), which coincided with deviations from setpoints in pH and DO. This deviation triggers corresponding control loops to maintain ideal conditions (Figure 3B).

Once the  $OD_{600}$  reached a saturating value, we chilled the culture to  $25$  °C for 30 min to allow incomplete plasmids to be finished before chilling to  $15$  °C for harvest.<sup>[49]</sup> We harvested cells by centrifugation, resulting in up to  $450$  g of wet cell paste (WCP) per 5 L of media. We expect that WCP can be stored at  $-80$  °C indefinitely without compromising the pDNA.

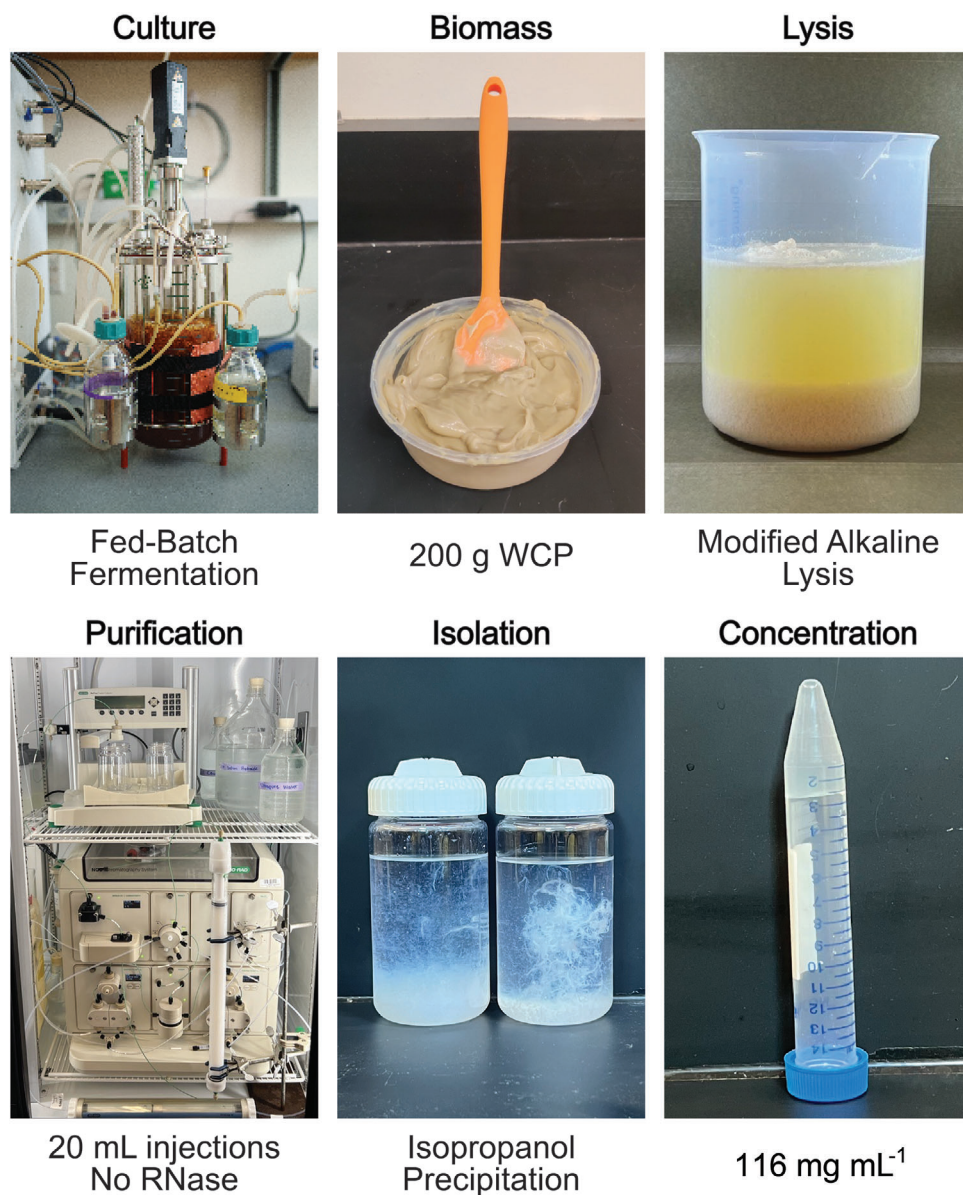


**Figure 1.** Process overview for bulk pDNA production and purification. Cultures are grown in a 7 L bioreactor vessel using a fed-batch fermentation protocol that produces  $\approx 100\text{--}400$  g of wet cell paste (WCP). Cells are lysed using a modified alkaline lysis protocol. pDNA is separated from RNA using AEX which is accomplished using a Bio-Rad NGC system equipped with a 193.9 mL column and a 90 mL injection loop. Purified DNA is concentrated using isopropanol precipitation and dissolved in TAE buffer or nuclease-free deionized water to a target concentration of  $100\text{ mg mL}^{-1}$ .

## 2.2. Primary Isolation

Alkaline lysis, the most common method to release pDNA from the bacterial cytoplasm, is often utilized for small-scale purifications in which a range of buffers, mixing strategies, and contact times can be used. Conversely, we found that purifying hundreds of grams of WCP demanded more stringent control over these parameters to maximize yields and minimize DNA damage.<sup>[36–39,48,50–52]</sup> In pursuit of a cost-effective and efficient purification technique that minimizes the need for specialized equipment, we focused on overcoming the major obstacles associated with large-scale alkaline lysis,

specifically addressing issues related to pDNA quality and lysate clarification.

To safeguard the target DNA from potential damage due to elevated pH, we incorporated glucose into the resuspension buffer, which was sufficient to maintain the pH below 12.5 throughout the lysis process.<sup>[53]</sup> Other potential lysis pitfalls that could reduce plasmid quality and make downstream purifications more difficult are shear-induced pDNA damage, fragmentation of genomic DNA, and local pH extremes, all of which result from either too vigorous or insufficient mixing. To overcome this challenge, industrial labs commonly employ specialized tanks and stirrers which are not commonly accessible.<sup>[35,51,52,54,55]</sup> However,

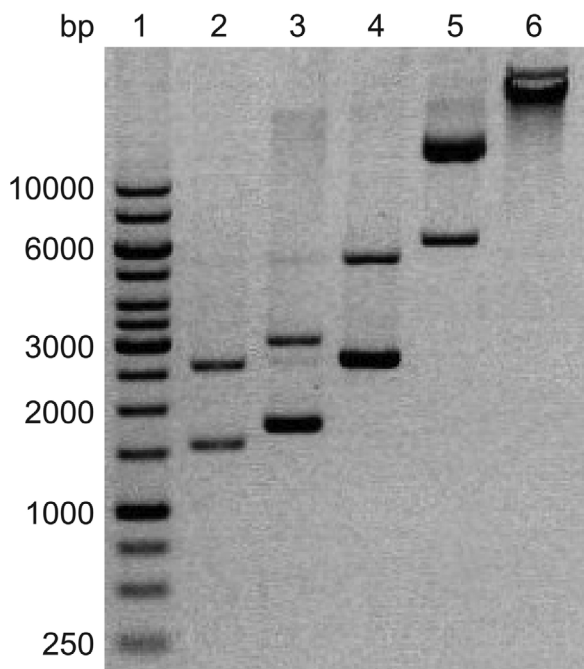


**Figure 2.** Comparison of purified plasmid samples. Gel electrophoresis analysis of the five different plasmids purified using our customized protocol on a 0.5% agarose gel. Lane 1: GeneRuler 1 kb molecular weight ladder, 2: pUC19 (2.686 kbp), Lane 3: pEGFP (3.075 kbp), Lane 4: pEYFP (5.045 kbp), Lane 5: pPIC11 (11 kbp), and Lane 6: Fos45 (45 kbp).

we have demonstrated that efficient lysis and neutralization can be accomplished in 5 L beakers by continuous stirring at 500 rpm for 5–10 min with a 2 in. octagon stir bar. During cell lysis, the viscosity of the solution increases significantly, preventing efficient mixing with the stir bar alone. To facilitate this step, a metal lab spatula is used to gently scrape the sides to ensure uniform exposure to the lysing solution.

We use contact times of 5 and 10 min for lysis and neutralization, respectively. Extended lysis and neutralization times do not increase yields and can introduce nicks into SC constructs that result in increased OC topology.<sup>[51]</sup> Following neutralization, we immediately remove precipitated debris through centrifugation. Additional resuspension and centrifugation of the debris pellets increases yields up to 10% which is significant on the gram scale (Figure 4A, lane 3).

In typical small-scale purification processes, the lysate is clarified with 0.2  $\mu\text{m}$  filters, which becomes time-consuming and costly when dealing with liters of lysed cells. In industrial processes, strategies such as tangential flow filtration (TFF), expanded bed adsorption, depth filtration, ultra/diafiltration, and the use of specialized filtration devices are employed to circumvent these challenges.<sup>[37,38,51,56–59]</sup> Here, we discovered that filtering the supernatant through cheesecloth sterilized with 70% ethanol followed by an ammonium acetate precipitation is sufficient to achieve the desired clarification of the lysate, circumventing the need for additional apparatuses and greatly reducing cost and time associated with 0.2  $\mu\text{m}$  filtration.

After passing the lysate through the cheesecloth, the crude DNA is concentrated using isopropanol precipitation and

dissolved in TE buffer (pH 8). Solid ammonium acetate is then added to precipitate proteins and large  $M_w$  RNA, and removed via centrifugation (Figure 4A, lanes 4 and 5). pDNA was then concentrated again through isopropanol precipitation and dissolved in a minimal volume of start buffer (10 mM Tris-HCl (pH 7.5), 1 mM EDTA, 0.62 M NaCl) for further purification to remove smaller  $M_w$  RNA (Figure 3A, lane 6). At each step of the isolation process, we use agarose gel electrophoresis (AGE) to assess the quality and yield of the pDNA (Figure 4A; and Figure S5, Supporting Information).

### 2.3. Anion Exchange Chromatography

Separation of the target plasmid from contaminating lower  $M_w$  RNA and proteins is accomplished using AEX. Typically, RNase digests, calcium chloride precipitations, or additional polishing steps (e.g., size exclusion chromatography) are needed to remove smaller  $M_w$  RNA, which significantly increases the purification time and cost.<sup>[36,38,48,39,59–60]</sup> To circumvent this obstacle, we developed a single stepwise sodium chloride gradient that successfully separates pDNA from RNA without the need for additional purification techniques or digests. While a step gradient is ideal for large-scale purifications, as it reduces separation time and buffer consumption, it can cause coelution of biomolecules due to sharp change in ionic strength.<sup>[61]</sup> To avoid this issue, we employed a series of continuous gradients to determine when contaminants and target DNA elute to design an optimized step gradient (Figures S6–S8, and S1, Supporting Information). To maximize the binding capacity of the column for our target DNA, we equilibrated the column using 0.6 M NaCl, which prevents adsorption of lower charge density impurities.<sup>[36]</sup>

We optimized the gradient using pUC19 (2.686 kbp) and a pre-packed 5 mL Q-Sepharose XL column (Cytiva), after which we scaled up to a 193.9 mL column packed with Q-Sepharose Fast Flow (FF) to increase throughput. When scaling up, we modified the gradient to accommodate changes in bed volume, sample volume, and resin to produce the step elution reported in Figure 4B, which shows an example chromatogram for the purification of pEYFP. Smaller  $M_w$  RNA elutes during the column wash at 0.62 M NaCl before pEYFP elutes at 0.7 M NaCl (Figure 4A, lane 7 and 8). Notably, this straightforward step gradient has proven effective in purifying all five plasmids without necessitating modifications.

Using AGE, we observe that our purified DNA samples exhibit a mixture of SC and OC isoforms, as evidenced by the presence of two distinct bands in the gel (Figures 2 and 4A). We quantify the fraction of each isoform using band intensity analysis in ImageJ, which we report below for the samples we characterize using bulk rheology. The fraction of SC versus OC plasmid varies across different preparations due to inadvertent single-stranded nicking of SC constructs that can occur during fermentation, primary isolation, and/or AEX purification. It is possible to separate these distinct isoforms which will be the focus of future studies.

Following purification, DNA is further concentrated using isopropanol precipitation, to achieve solutions hundreds of times above the overlap concentration  $c^*$ . We observe that redissolving the DNA pellet at concentrations above 10 mg mL<sup>-1</sup> often results in visible translucent regions with more gel-like properties than

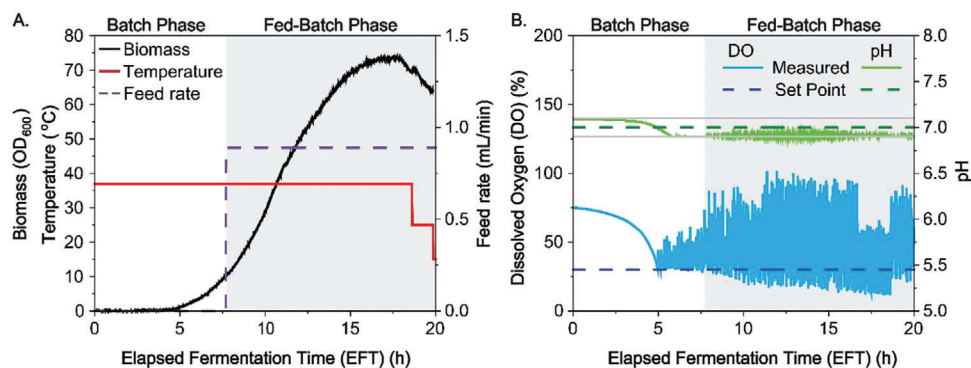


**Figure 3.** Typical data from a 7 L fed-batch fermentation of *E. coli* DH5 $\alpha$  cells producing a 5.045 kbp pEYFP plasmid. A) Time course showing biomass (solid black line), temperature (solid red line), and nutrient feed rate (dashed purple line) monitored during fermentation. Temperature setpoint was 36.9 °C and the feed rate was 0.89 mL min<sup>-1</sup>. B) Time course of dissolved oxygen (DO, solid light blue line) and pH (solid light green line) monitored during fermentation. DO setpoint (dashed dark blue line) was 30% and was controlled by oxygen supplementation. pH set point (dashed dark green line) was 7.0 and was controlled with ammonium hydroxide and phosphoric acid with a dead band of 0.1 (solid gray lines). Gray regions in each plot denote the fed-batch phase which was initiated at 7.7 h using a constant feed rate calculated based on a batch phase maximum specific growth rate ( $\mu_{\max} = 0.67$  h<sup>-1</sup>). The fermentation process was completed at Elapsed Fermentation Time (EFT) 20.7 h, yielding 190 mg L<sup>-1</sup> and a theoretical yield of 950 mg of pEYFP for the run.

the surrounding solution. To homogenize the solution, we incubate DNA in the desired final buffer (e.g., TE, TAE, or DI) for  $\geq 48$  h at 4 °C. We then gently mix samples with a sterile 22G needle then centrifuge, repeating this process up to three times, which we find is sufficient to produce a visibly homogenized solution. We incubate the homogenized sample at 4 °C for another 48 h before measuring the concentration in triplicate at different points in the sample using a nano spectrophotometer and confirm using AGE. This process reliably results in DNA samples with concentrations up to 116 mg mL<sup>-1</sup>.

#### 2.4. Bulk Rheology

A primary goal of developing this process is to enable robust bulk rheology measurements of monodisperse solutions of highly overlapping polymers of different topologies, to fill a major need in the polymers and materials community. To demonstrate achievement of this goal, we perform bulk linear oscillatory rheology measurements for pEYFP and pPIC11 over a range of concentrations and multiple topologies. For all cases, we measure linear elastic and viscous moduli,  $G'(\omega)$  and  $G''(\omega)$ , over 5 decades

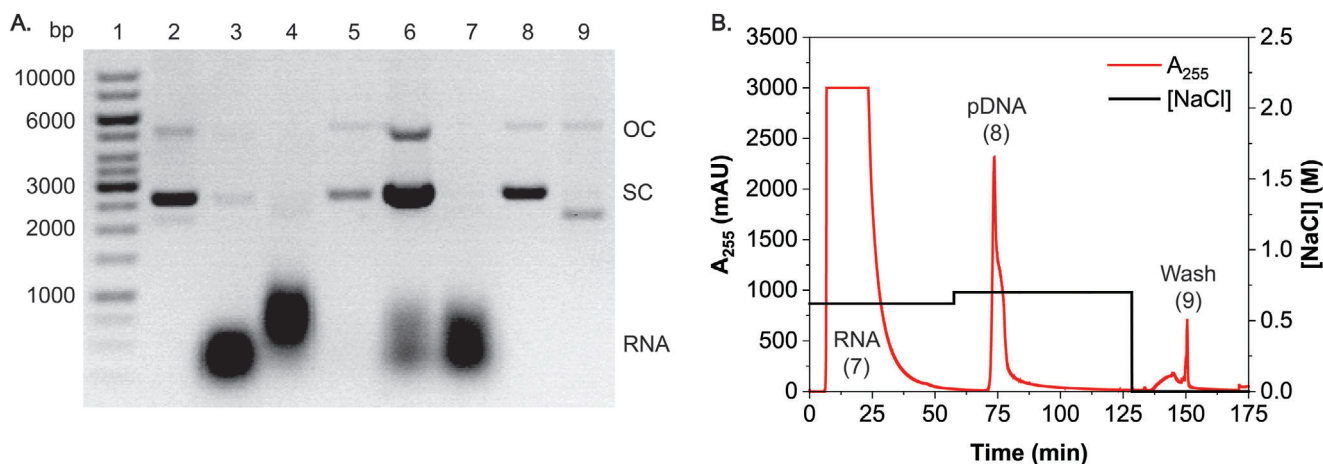


**Figure 4.** Purification of the crude DNA solution. A) Gel electrophoresis analysis of purification fractions on a 0.5% agarose gel. Lane 1: GeneRuler 1 kb molecular weight ladder, Lane 2: 0.1  $\mu$ g of commercial pEYFP, Lane 3: pDNA and RNA recovered from debris pellet washes, Lane 4: Ammonium acetate precipitation pellet containing larger  $M_w$  RNA, Lane 5: Ammonium acetate precipitation supernatant containing crude pDNA, Lane 6: Crude DNA solution containing pDNA and lower  $M_w$  RNA, Lane 7: Peak 1 containing RNA eluting during the 0.62 M NaCl column wash prior to elution, Lane 8: Peak 2 containing purified pEYFP eluting at 0.70 M NaCl, and Lane 9: Peak 3 containing denatured plasmid eluting during the 1 M NaOH wash. B) pDNA purification using anion exchange chromatography in a 193.9 mL column (395 mm X 25 mm) packed with Q-Sepharose FF using an optimized gradient. The flow rate was 10 mL min<sup>-1</sup> with washing/elution buffers containing 10 mM Tris-HCl (pH 7.5), 1 mM EDTA, and NaCl at the concentration shown by the solid black line. The sample injection volume was 15 mL of crude pEYFP solution, corresponding to a total 188.7 mg of nucleic acid (DNA, RNA) loaded onto the column. Purification was monitored by measuring the absorbance at 255 nm (solid red line). Peaks corresponding to RNA and DNA are labeled as determined by gel electrophoresis shown in (A).

of frequency, greatly expanding the dynamic range above the 3 decades previously reported for DNA solutions.<sup>[9,11,62,63]</sup> We note that due to concerns of shear induced linearization of Fos45, we chose to delay its study until we could ensure its quality.

We performed rheological measurements of pEYFP (5.045 kbp) at 4 different concentrations from 10 to 80 mg mL<sup>-1</sup> (Figure 5). Considering the fraction of SC and OC DNA that comprise the solution (≈37% SC and ≈63% OC), these concentrations range from ≈4.2c\* to ≈34c\*, which spans from below to well above the nominal entanglement concentration, c<sub>e</sub> ≈6c\* for linear chains, and exceeds the previously reported maximum concentration of ≈12c\* for bulk rheology measurements on circular DNA.<sup>[9,24,63]</sup> Beyond the increased dynamic range we achieve, our systems have a higher fraction of supercoiled DNA compared to most previous studies.<sup>[18,24,63,64]</sup> Advantageously we also observe no discernible linear contaminants, which has only been reported a small number of times.<sup>[18,24,63,64]</sup> Comparison of our unmodified pure pDNA samples with linearized counterparts confirms that the two bands present in the solutions used for bulk rheology are SC and OC isoforms and not linear contaminants (Figure S9, Supporting Information).

By accessing this new region of the phase space, we observe several regimes of distinct rheological properties, including a low-frequency elastic plateau, a crossover at a frequency ω<sub>c</sub> to a viscous-dominated regime in which G'' > G', followed by an additional high frequency crossover at ω<sub>2</sub> to an elastic-dominated regime, with G' > G''. Notably this behavior is distinct from the bulk rheological behavior previously reported for linear and circular DNA, most of which display terminal regime scaling at low frequencies and none of which display a high frequency crossover beyond the elastic plateau.<sup>[9,18,63,65]</sup> In fact, the lower concentration data (10 and 20 mg mL<sup>-1</sup>) display frequency dependence much more akin to that of semiflexible actin filaments which exhibit a rubbery plateau at low frequencies and high frequency scaling regime in which G'' > G' and G'' ≈ G' ≈ ω<sup>x</sup> where x = 3/4 – 7/8.<sup>[66]</sup> This feature may be a fingerprint of the supercoiled DNA which likely has reduced flexibility due to its twist and writhe.<sup>[20,30,64,67]</sup> Additionally, interactions between rings and supercoiled constructs, such as interpenetration, may introduce additional constraints that suppress terminal regime dynamics. In support of this conjecture, previous microrheology studies on semidilute solutions of SC and OC DNA showed evidence of entanglement-like dynamics at concentrations well below c<sub>e</sub> suggestive of stronger than expected constraints.<sup>[64,67]</sup>

While direct comparison is not possible as there are no rheology experiments (to our knowledge) reported for circular or SC DNA of similar size to pEYFP (5 kbp), one previous study used optical tweezers microrheology to study the rheological properties of 8c\* solutions of 6 kbp DNA with similar SC:OC ratio to our system (37%:63%).<sup>[68]</sup> Like our results for the 4.8c\* (10 mg mL<sup>-1</sup>) solution, this study reported G' and G'' values that increase with frequency from G' ≈ 0.1 Pa and G'' ≈ 0.05 Pa to G' ≈ 0.8 Pa and G'' ≈ 1 Pa over a frequency range ω = 1–100 rad s<sup>-1</sup>. They also identified a low-frequency crossover to G' > G'' at ω<sub>c</sub> ≈ 2 rad s<sup>-1</sup>, similar to our data and observe a lack of terminal regime dynamics across the measurable frequency ranges.

To further validate our results and demonstrate the ability to greatly expand the measurable dynamic range, we produced

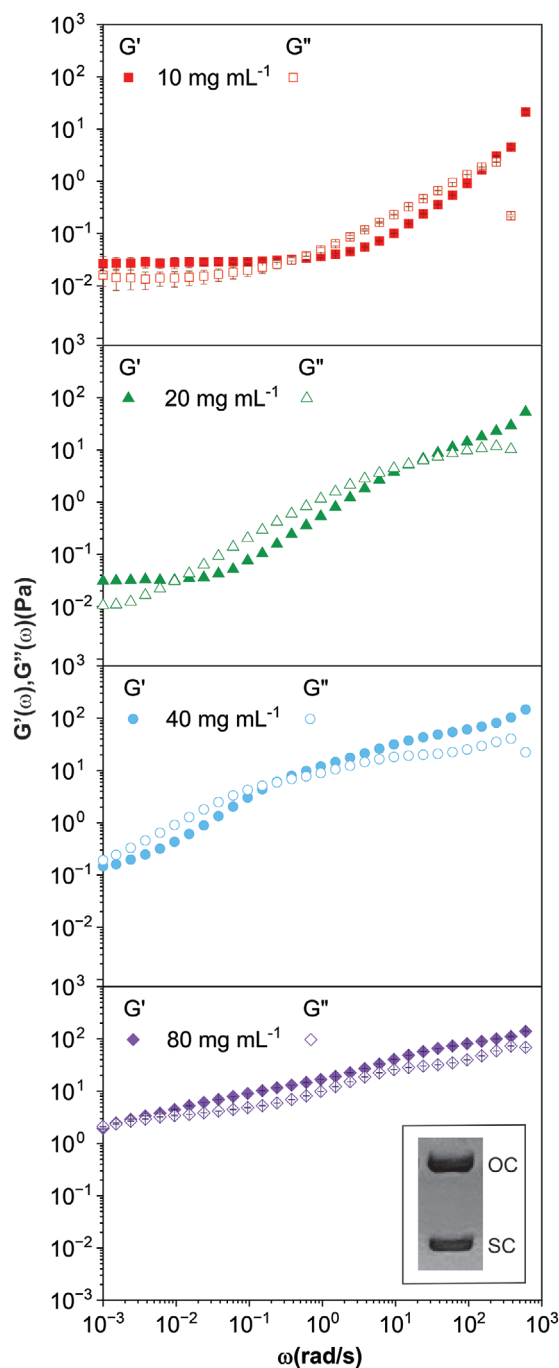


**Figure 5.** Bulk linear oscillatory rheology measurements of pEYFP at four different concentrations. Linear viscoelastic moduli,  $G'(\omega)$  (storage modulus, closed symbols) and  $G''(\omega)$  (loss modulus, open symbols) versus angular frequency,  $\omega$ , for 10 mg mL<sup>-1</sup> (red squares), 20 mg mL<sup>-1</sup> (green triangles), 40 mg mL<sup>-1</sup> (blue circles), and 80 mg mL<sup>-1</sup> (purple diamonds) pEYFP solutions. Samples contain 63% OC and 37% SC pEYFP. Data shown for 10 and 80 mg mL<sup>-1</sup> samples are an average over 2 independent measurements and the error bars represent standard error. All measurements were performed on a TA Instruments DHR-3 rheometer with parallel plate geometry. Image depicted in bottom right shows agarose gel electrophoresis analysis of the sample used for the reported data highlighting the different isoforms (SC and OC) of pEYFP.

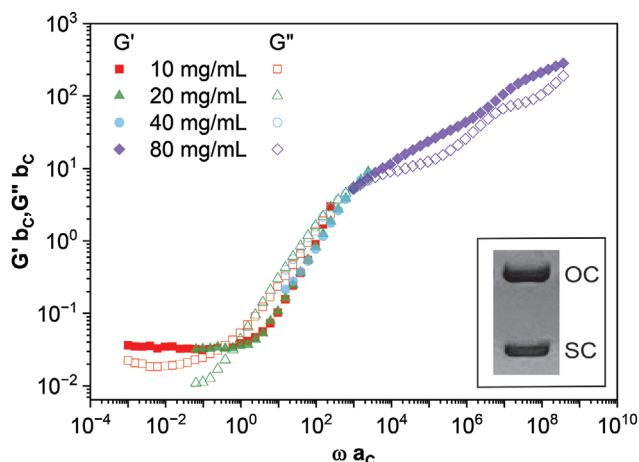


**Figure 6.** Master curve of linear viscoelastic properties for pEYFP. Linear viscoelastic moduli,  $G'(\omega)$  (storage modulus, closed symbols) and  $G''(\omega)$  (loss modulus, open symbols) for each concentration [10 mg mL<sup>-1</sup> (red squares), 20 mg mL<sup>-1</sup> (green triangles), 40 mg mL<sup>-1</sup> (light blue circles), and 80 mg mL<sup>-1</sup> (purple diamonds)] are shifted horizontally and vertically relative to the 10 mg mL<sup>-1</sup> sample by respective factors  $a_c$  and  $b_c$ . This process generates a single time-concentration superposition master curve that spans 12 decades in frequency and 4 decades in modulus values. Image depicted in bottom right shows agarose gel electrophoresis analysis of the sample used for the reported data highlighting the different isoforms (SC and OC) of pEYFP.

a time-concentration superposition master curve (Figure 6). By shifting  $G'(\omega)$  for the different concentrations such that the  $\omega_c$  and  $G'(\omega_c)$  values in each data set align, we observe collapse into a single master curve that spans 12 decades of frequency. This master curve captures all of the features discussed above, from the low-frequency entanglement plateau to the high-frequency  $G' > G''$  regime, as well as two distinct crossovers,  $\omega_c$  and  $\omega_2$ . The shifting factors plotted as a function of concentration are shown in Figure S10 (Supporting Information). It is possible at very low frequencies that a crossover to terminal behavior would be reached, but attempts to collect measurements on a 5 mg mL<sup>-1</sup> sample of pEYFP with the 180  $\mu$ L sample volume used for data reported in Figure 5 were unsuccessful. Previous bulk rheology studies for OC DNA at lower concentrations have also not observed terminal behavior.<sup>[24,63]</sup> Additionally, microrheology experiments on semidilute blends of OC and SC DNA reported entanglement-like dynamics at concentrations well below the critical entanglement concentration, suggestive of stronger than expected constraints.<sup>[20,24,63]</sup> These studies suggest that terminal regime behavior may be hard to reach in pure ring solutions.

A significantly more supercoiled sample of pEYFP (79% SC vs 37% SC) showed more terminal flow like behavior at 5 and 10 mg mL<sup>-1</sup> where  $G' < G''$  at all frequencies (Figure 7). Both samples exhibit terminal flow scaling as expected ( $G' \approx \omega^2$  and  $G'' \approx \omega^1$ ) with a modest degree of polymer overlap (Figure 7). These concentrations correspond to  $1.6c^*$  to  $3.2c^*$ , respectively, which is well below the entanglement regime. The zero-shear viscosities for these two samples are  $\approx 0.04$  and  $\approx 0.09$  Pa s which align with expected scaling  $\eta \approx c$ . The crossover into the terminal like regime of the more supercoiled pEYFP is in agreement

with the suggestion that supercoiling enhances plasmid mobility.<sup>[20]</sup>

Due to the relatively dilute concentrations the rheometer approached its torque limit when studying the 5 mg mL<sup>-1</sup> 79% SC pEYFP solution, requiring us to omit data at low frequencies. Fortunately, the scale of these preparations allowed for large sample volumes (1 mL) to be used, which greatly increased the range of measurable frequencies versus the first samples using 180  $\mu$ L (Figure 7). At 5 mg mL<sup>-1</sup> using a 1 mL sample, we could reliably make measurement of  $G'$  down to 0.15 rad s<sup>-1</sup>, and at 10 mg mL<sup>-1</sup>  $G'$  could be measured to 0.1 rad s<sup>-1</sup> representing an order of magnitude improvement versus the 180  $\mu$ L sample. This clearly demonstrates the advantage of both the concentration and scale that this method provides.

Beyond the terminal regime, the high-frequency crossover to  $G' > G''$  is often an indicator of the onset of glassy dynamics for entangled polymers, which has been suggested to underlie some features of concentrated solutions of ring polymers.<sup>[28,69–71]</sup> However, rather than  $G'$  reaching another plateau and  $G''$  decreasing as is seen in traditional glass transitions in which the polymers are arrested, here we see that both viscoelastic moduli continue to increase. Based on previous studies, we conjecture that this effect may be due to heterogeneous microscale dynamics arising from regions of dynamically arrested polymers within a bath of faster moving polymers.<sup>[28,69–71]</sup> With the ability to produce large quantities of this DNA and similar SC and OC plasmids, we plan to explore this rich emergent behavior in depth in future studies.

To further demonstrate the efficacy of our process for improved access to bulk rheology measurements, we prepare concentrated solutions of pPIC11 (11 kbp), which has been previously studied.<sup>[15,24]</sup> We perform linear oscillatory measurements

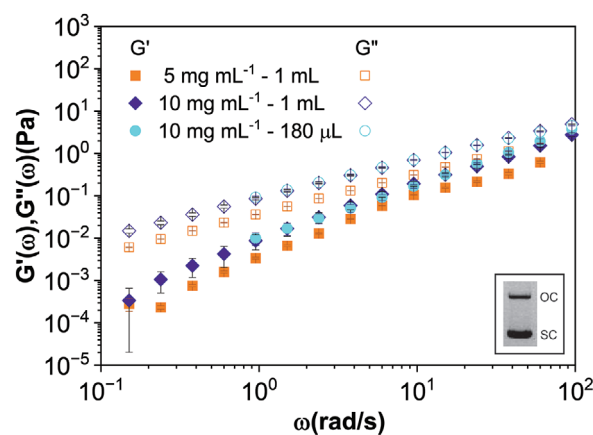


**Figure 7.** Bulk linear oscillatory rheology measurements on pEYFP with larger sample volumes. Linear viscoelastic moduli,  $G'(\omega)$  (storage modulus, closed symbols) and  $G''(\omega)$  (loss modulus, open symbols) versus angular frequency,  $\omega$ , for 5 mg mL<sup>-1</sup> pEYFP using 1 mL sample volume (orange squares) and 10 mg mL<sup>-1</sup> pEYFP using a 1 mL (dark purple diamonds) and 180  $\mu$ L (cyan circles) sample volume. The ring solutions contain 21% OC and 79% SC. Data shown is an average over 3 independent measurements and the error bars represent standard errors. All measurements were performed on a TA Instruments DHR-3 rheometer with parallel plate geometry. Image depicted in bottom right show agarose gel electrophoresis analysis of the sample used for the reported data highlighting the different isoforms (SC and OC) of pEYFP.

on pPIC11 solutions contain  $\approx 85\%$  SC and  $15\%$  OC DNA at concentrations of  $25$ ,  $50$ , and  $116 \text{ mg mL}^{-1}$  which correspond to  $\approx 15c^*$ ,  $\approx 30c^*$ , and  $\approx 69c^*$ , respectively. These concentrations span from comparable to well above the maximum previously studied concentration of  $\approx 11c^*$  for circular DNA.<sup>[9,24,63]</sup> Moreover, these previous studies were performed on solutions with minimal to no supercoiled content due to the difficulty in preserving supercoiling in bulk purification methods.<sup>[15]</sup> The  $85\%$  supercoiling achieved with our methods represents a major advance in DNA engineering, and  $99\%$  SC samples can be achieved with modern AEX resins.

As shown in Figure 8A, we do not observe a transition to terminal regime scaling for even the lowest concentration, consistent with previous studies on concentrated ring polymers.<sup>[13,16,17,25,63,72–74]</sup> We also do not observe a clear elastic plateau regime; rather,  $G'(\omega)$  follows approximate power-law scaling for all concentrations. These features are similar to those reported for previous bulk rheology measurements of OC pPIC11 DNA solutions at  $\approx 11c^*$ , further validating the integrity of the DNA material we have produced. The relatively larger magnitudes of  $G'$  and  $G''$  for our measurements compared to previous work, may be a result of not only the concentration, but also interactions between SC and OC DNA that possibly enhance constraints compared to pure ring solutions.<sup>[20]</sup>

As the majority of rheology studies on DNA have focused on linear DNA, we sought to demonstrate the ability of our methods to also produce high concentrations and large volumes of previously studied linear DNA.<sup>[75]</sup> To this end, we prepare linear pPIC11 by digesting circular pPIC11 with the restriction endonuclease, BamHI, that cleaves the plasmid at a single location to produce a solution of  $100\%$  linear pPIC11 (Figure S2, Supporting Information) (see the Experimental Section). Our bulk rheology measurements for  $25$  and  $50 \text{ mg mL}^{-1}$  linear pPIC11 display regions  $G'$  is independent of frequency, with values of  $G^0 \approx 226 \pm 2 \text{ Pa}$  and  $G^0 \approx 810 \pm 9 \text{ Pa}$  (Figure 8B). This concentration dependence is consistent with a scaling relation  $G^0 \approx c^{(1.9 \pm 0.3)}$  which aligns with predicted and experimentally observed scaling exponents that range from  $2$  to  $2.2$  for entangled linear polymers.<sup>[62,76–79]</sup> Of note, while the linear and circular solutions are at the same mass concentration, the relative overlap (i.e.,  $c/c^*$ ) of the linear DNA is much higher due to their larger radius of gyration compared to OC and SC DNA and the scaling  $c^* \approx R_g^{-3}$ . Specifically,  $25$  and  $50 \text{ mg mL}^{-1}$  linear DNA solutions correspond to  $\approx 200 c/c^*$  and  $\approx 400 c/c^*$ , which exceed the previously reported maximum overlap for linear DNA of  $c/c^* \approx 89$ .<sup>[9]</sup> The one previous study (to our knowledge) that examined the rheology of linear pPIC11 used optical tweezers microrheology to measure  $G'(\omega)$  and  $G''(\omega)$  for semidilute solutions ( $c \approx 4.8c^*$ ), reporting terminal regime scaling across the entire frequency range of  $\approx 5\text{--}100 \text{ rad s}^{-1}$ . We are unable to directly compare these previous results due to limits on the sensitivity and torque limit of our bulk rheometer. The detailed interpretation of the rheological behavior shown in Figures 5–8 is the subject of future works as more preparative scale techniques need to be developed, e.g., the separation of OC and SC DNA and limiting shear induced linearization of Fos45, to produce samples of sufficient purity, scale, and concentration for detailed study. However, we hope the results presented give new insight into the behavior of highly concentrated ring solutions.

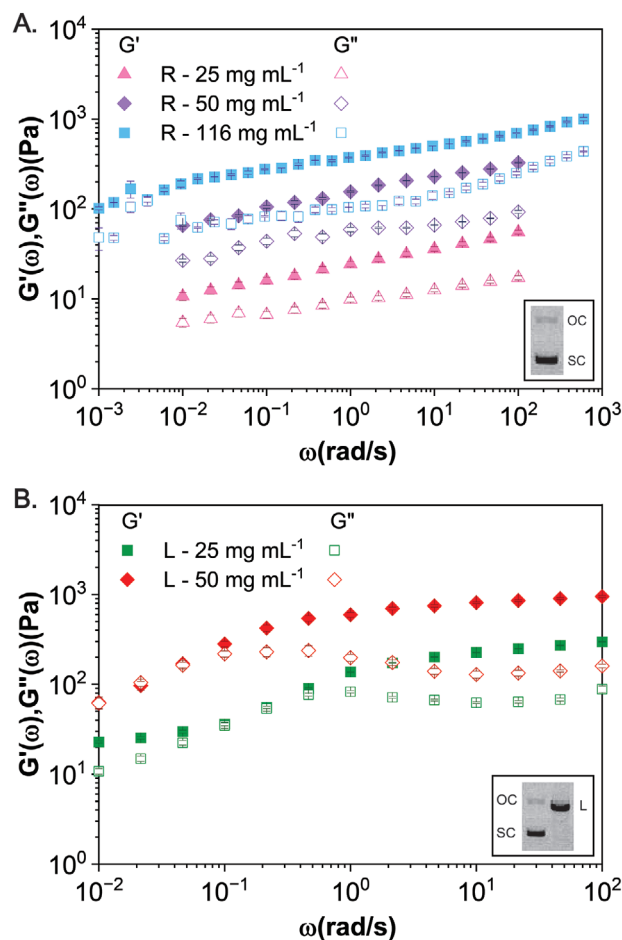


**Figure 8.** Bulk linear oscillatory rheology measurements of solutions of ring (R) and linear (L) pPIC11. Linear viscoelastic moduli,  $G'(\omega)$  (storage modulus, closed symbols) and  $G''(\omega)$  (loss modulus, open symbols) versus angular frequency,  $\omega$ , of R and linear L) pPIC11 solutions. A) Ring pPIC11 solutions at  $25$ ,  $50$ , and  $116 \text{ mg mL}^{-1}$ . B) Linear pPIC11 solutions at  $25$  and  $50 \text{ mg mL}^{-1}$ . The ring solutions contain  $15\%$  OC and  $85\%$  SC. Data shown is an average of 2 independent measurements for the R –  $116 \text{ mg mL}^{-1}$  sample, 24 independent measurements for the R –  $25 \text{ mg mL}^{-1}$ , R –  $50 \text{ mg mL}^{-1}$ , and L –  $25 \text{ mg mL}^{-1}$  samples, and 8 independent measurements for the L –  $50 \text{ mg mL}^{-1}$  sample. The error bars represent standard errors. All measurements were performed on a TA Instruments DHR-3 rheometer with parallel plate geometry. Images depicted in bottom right show agarose gel electrophoresis analysis of the sample used for the reported data highlighting the different isoforms (SC, OC, and L) of pPIC11.

### 3. Conclusions

Here, we present a robust methodology for the bulk production and purification of circular DNA, employing simple and scalable techniques. The total cost for producing and purifying  $100$  grams of WCP amounts to  $\approx \$324$ , inclusive of all consumables, reagents, and solvents utilized throughout the process, and requires  $\approx 10$  h of labor producing  $\approx 230 \text{ mg}$  of pDNA. Single bioreactor runs can yield more than  $400 \text{ g}$  WCP, allowing access to gram-scale amounts of pDNA. Simple comparison of the rheology of linear, OC, and SC DNA obtained through this method provides an intriguing insight into the dynamics of ring

polymers. Further study of these phenomena will not only provide invaluable insight into the laws which govern ring polymers, but also shed light on the behavior of DNA in the nucleus which cannot undergo traditional reptation due to the relative lack of polymer “ends.” Our future endeavors will focus on expanding our repository of reliably purified constructs, e.g., Fos45, and further enhancing yields through the adoption of more intricate fermentation protocols as well as obtaining and studying pure samples of SC and OC DNA. The approach harbors the potential to revolutionize the utilization of DNA as a commodity and model polymer, addressing prominent challenges within the realms of polymer science and materials engineering. Moreover, it dramatically enhances the accessibility of DNA-based research, potentially ushering in a new era of innovation and exploration in this field.

#### 4. Experimental Section

Below the key methods used and the data reported are described. A more detailed description of these methods along with recipes for all solutions used can be found in the Supporting Information. Information was also provided on preparing and operating the bioreactor along with the optimization process for AEX.

**Fed-Batch Fermentation:** For pUC19 (2.686 kbp), pUCBB-pT7-eGFP (pEGFP, 30.075 kbp), pUCP20T-eYFP (pEYFP, 5.045 kbp), and Fos45 (45 kbp), DH5 $\alpha$  *E. coli* cells were transformed before each run to produce inocula. For pPIC11, glycerol stocks of DH5 $\alpha$  *E. coli* cells containing pIC11 (11 kbp) were used to prepare inocula. All inocula were grown at 30 °C with shaking at 300 rpm in LB media supplemented with an appropriate antibiotic (ampicillin for pUC19, pEGFP, pEYFP, and pPIC11 at 100  $\mu\text{g mL}^{-1}$  and chloramphenicol for Fos45 at 35  $\mu\text{g mL}^{-1}$ ). Fermentations were grown in a semidefined media containing the appropriate antibiotic (same as above) using a simple fed-batch protocol adapted from Carnes et al.<sup>[49]</sup> A bioreactor Applikon ez2-control system equipped with a 7 L vessel was used to monitor and control culture conditions throughout fermentations. Cultures were aerated at 2 vessel volumes per min (VVM) and oxygen supplementation was initiated automatically to maintain a dissolved oxygen (DO) setpoint of 30% air saturation. pH was controlled at 7.0  $\pm$  0.1 through the automatic addition of ammonium hydroxide (28%–30%) or phosphoric acid (25%). The temperature setpoint was 36.9 °C and was controlled by active heating and cooling of the vessel. Real-time monitoring of culture growth was accomplished using an inline optical density (OD<sub>600</sub>) internal reflectance probe (BugLab). Upon reaching the target OD<sub>600</sub> of 10  $\pm$  2, the fed-batch phase was initiated by adding a chemically defined feed medium according to a predetermined linear rate which was calculated using the maximum specific growth rate ( $\mu_{\text{max}}$ ) of the batch phase. Cultures were grown at 36.9 °C for an average of 20 h and chilled to 25 °C for 30 min before being cooled to 15 °C for harvest. Wet cell paste (WCP) was stored at –80 °C until lysis and purification. WCP was stored for up to 4 years without any noticeable changes in plasmid quality or quantity. Volumetric (mg pDNA per L of culture) and specific (mg pDNA per g WCP) plasmid yields were determined at the end of each run using commercially available miniprep kits (ThermoFisher GeneJet Mini Prep).

**Primary Plasmid Isolation:** Cells were harvested by centrifugation and lysed using a modified alkaline lysis protocol that was developed, as detailed in the Supporting Information, along with recipes for all necessary buffers. Briefly, frozen cell pellets were resuspended to a total volume of 15 mL of resuspension buffer (25 mM Tris-HCl (pH 8), 10 mM EDTA, 50 mM glucose) per gram of WCP in a plastic 5 L Corning beaker. Cell resuspension was facilitated by stirring at 500 rpm on a stir plate (IKA RCT Basic) using a 2 in. octagon stir bar. Lysis was accomplished by the addition of 1 mL alkaline lysis buffer (0.2 M NaOH, 1% SDS) per mL of resuspended cells. The lysed cell solution was agitated at 500 rpm for 5 min at room temperature, after which the solution was neutralized by adding 1 mL of neutralization buffer (3 M potassium acetate) per mL of

resuspended cells which produced a flocculent containing genomic DNA and cellular debris. Neutralization was carried out at room temperature for 10 min with stirring at 500 rpm before precipitated debris was removed by centrifugation (10 000 g, 4 °C, 30 min). To increase yields, debris pellets were washed with a 1:1:1 ratio of resuspension buffer: alkaline lysis buffer: neutralization buffer. Debris is removed again by centrifugation as described above.

The combined supernatant was passed through 16 layers of cheese cloth (Grade 90, Arkwright LLC) and a mesh tea strainer (7/8 in., Little Cook since 1995) into 5 L Corning beakers. DNA was precipitated through the addition of 0.6 volumes of isopropanol. Solutions were gently mixed using a spatula and incubated at –20 °C for 16 h. DNA was harvested by centrifugation (12 000 g, 4 °C, 60 min) and dissolved in TE buffer (10 mM Tris-HCl (pH 8), 1 mM EDTA) before solid ammonium acetate was added to a final concentration of 3 M. Once dissolved, this solution was incubated on ice for 20 min, after which precipitated proteins and larger molecular weight RNA were removed by centrifugation (10 000 g, 4 °C, 20 min). DNA was then concentrated using the isopropanol precipitation protocol described above. DNA pellets were washed with 70% ethanol and dried before being dissolved in the start buffer (10 mM Tris-HCl (pH 7.5), 1 mM EDTA, 0.62 M NaCl) to yield a crude DNA solution in which the major contaminant is lower molecular weight RNA.

**Anion Exchange Chromatography—Stationary Phase:** For large-scale purifications, a 500 mm  $\times$  25 mm inner diameter column (Bio-Rad Econo Alpha Medium Pressure Chromatography Columns) was packed with Q-Sepharose Fast Flow (Cytiva), a strong anion exchanger made of highly cross-linked, 6% agarose beads (90  $\mu\text{m}$ ) containing quaternary amine groups. The column was packed to a final bed height of 39.5 cm with a corresponding bed volume of 193.9 mL. The column and resin were used following manufacturer protocols.

**Anion Exchange Chromatography—Mobile Phase:** The mobile phase was made of a TE buffer system in which buffer A was 10 mM Tris-HCl (pH 7.5), 1 mM EDTA and buffer B was 10 mM Tris-HCl (pH 7.5), 1 mM EDTA, 2 M NaCl. The absorbance of the eluate was monitored at 255 nm and all purifications were carried out at 4 °C. Unless stated otherwise, the following gradient was used for large-scale purifications, 0.62 M NaCl for 55 min followed by 0.70 M NaCl for 70 min. Flow rate was 10 mL min<sup>–1</sup>, and the injection volume was 15–30 mL, dependent on concentration of crude DNA solution. The optimal injection volume for each crude DNA solution was determined by analyzing the column wash peak to maximize sample load while avoiding plasmid loss. The optimal injection volume is defined as the maximum volume that can be loaded without detection of pDNA in the column wash. All samples were characterized using agarose gel electrophoresis (AGE) and UV–Vis absorption spectroscopy. Between purifications, the column was washed with 1 M NaOH until the absorbance at 255 nm returned to baseline before regenerating the column with 2 M NaCl.

**pDNA Concentration and Homogenization:** To concentrate purified pDNA samples, 0.6–1 volume of isopropanol was added. Bottles were gently inverted six times. Solutions were then incubated either at room temperature for 2 h or –20 °C for 24 h. Precipitated DNA was then harvested by centrifugation (12 000 g, 4 °C, 40 min). Pellets were then washed with 70% ethanol and reformulated by centrifugation (12 000 g, 4 °C, 40 min). To homogenize the solution, DNA was incubated in the desired final buffer (TAE or nuclease-free water) for at least 48 h at 4 °C. Then gently mix samples with a sterile 22G needle and centrifuge, repeating the process up to three times, which was found sufficient to produce a visibly homogenized solution. The homogenized sample was incubated at 4 °C for another 48 h before measuring the concentration in triplicate using a nanospectrophotometer and AGE. Solutions were diluted as needed to ensure measurements were within the detection limits of the instrument. A dilution factor of five was not exceeded and homogenization of the diluted samples followed the same procedure as above but 24 h incubation periods were used instead of 48 h.

**Large-Scale Linearization of pPIC11:** pPIC11 was linearized using BamHI in 1X BamHI buffer diluted with nuclease-free water. The final concentration of pPIC11 and BamHI in the digest were 3 mg mL<sup>–1</sup> and 200 U mL<sup>–1</sup>, respectively, corresponding to 0.1 U of BamHI per  $\mu\text{g}$  of pDNA.

Restriction digests were conducted at 37 °C for 16 h after which EDTA (240  $\mu$ L, 0.5 M) was added to a final concentration of 5 mM to inactivate BamHI. Isopropanol precipitation was used to concentrate the linearized plasmid and remove digest buffer. The DNA pellet was dissolved in nuclease-free water and the sample was homogenized using the same procedure described above. Success of digest was determined using AGE (Figure S5, Supporting Information). For the data reported in Figure 8, 18 mg of pPIC11 was linearized which required 1800 U of BamHI. BamHI was purchased through Thermo Fisher at \$0.03 per unit resulting in a final cost of \$62.6 for the enzymes used in this work.

**Rheological Experiments:** All rheological measurements were conducted using a DHR-3 rheometer (TA-Instruments) with a 40 mm stainless steel parallel plate and fixed temperature of 22 °C. Highly concentrated stock solutions of pDNA were diluted appropriately with nuclease-free water to achieve target concentrations. Samples were homogenized using a FlackTek mixer. For small volume measurements, 180  $\mu$ L of sample was pipetted onto the bottom plate and the upper geometry was slowly lowered until the gap was filled. For large sample volumes, 1 mL of sample was pipetted onto the bottom plate and the upper geometry was slowly lowered until the gap was filled. To prevent evaporation of sample during tests, mineral oil was placed around the edges of the geometry. Amplitude sweeps were performed at multiple frequencies to confirm that frequency sweeps were conducted within the linear viscoelastic region (Figure S11, Supporting Information). All frequency sweeps shown were conducted at 10% strain to determine the linear elastic and viscous moduli  $G'(\omega)$  and  $G''(\omega)$ . At least two runs were performed for all data shown, and error bars represent standard errors. Data from frequency sweeps performed on each sample were overlaid to demonstrate consistency between measurements and show that no evaporation, aging, or oil dispersion was observed throughout the course of the experiments (Figures S12–S15, Supporting Information).

## Supporting Information

Supporting Information is available from the Wiley Online Library or from the author.

## Acknowledgements

N.J.O. would like to acknowledge the support from CIBBR (NIH, P20GM113131), NH Biomade (NSF, No. IIA 1757371), and the NSF CAREER award (DMR 2340569). R.M.R.A. acknowledged support from AFOSR (No. FA9550-21-1-0361) and NIH NIGMS (No. 2R15GM123420-02).

## Conflict of Interest

The authors declare no conflict of interest.

## Data Availability Statement

The data that support the findings of this study are available from the corresponding author upon reasonable request.

## Keywords

bioreactors, circular polymers, plasmid DNA, rheology, unimolecular polymers

Received: April 17, 2024  
Revised: June 10, 2024  
Published online: July 4, 2024

- [1] D. Wang, P. Liu, D. Luo, *Angew. Chem., Int. Ed.* **2022**, *61*, 202110666.
- [2] F. Li, J. Tang, J. Geng, D. Luo, D. Yang, *Prog. Polym. Sci.* **2019**, *98*, 101163.
- [3] C. Wang, J. Zhang, *ACS Appl. Bio. Mater.* **2022**, *5*, 1934.
- [4] D. Wang, Y. Hu, P. Liu, D. Luo, *Acc. Chem. Res.* **2017**, *50*, 733.
- [5] F. Li, D. Lyu, S. Liu, W. Guo, *Adv. Mater.* **2020**, *32*, 1806538.
- [6] O. Okay, *J. Polym. Sci., Part B: Polym. Phys.* **2011**, *49*, 551.
- [7] H. Budharaju, A. Zennifer, S. Sethuraman, A. Paul, D. Sundaramurthi, *Mater. Horiz.* **2022**, *9*, 1141.
- [8] R. Bandyopadhyay, A. Sood, *Pramana* **2002**, *58*, 685.
- [9] S. Banik, D. Kong, M. J. San Francisco, G. B. McKenna, *Macromolecules* **2021**, *54*, 8632.
- [10] L. Bravo-Anaya, M. Rinaudo, F. Martínez, *Polymers* **2016**, *8*, 51.
- [11] R. E. Teixeira, A. K. Dambal, D. H. Richter, E. S. G. Shaqfeh, S. Chu, *Macromolecules* **2007**, *40*, 2461.
- [12] C. M. Schroeder, *J. Rheol.* **2018**, *62*, 371.
- [13] K. Regan, S. Ricketts, R. Robertson-Anderson, *Polymers* **2016**, *8*, 336.
- [14] A. R. Klotz, B. W. Soh, P. S. Doyle, *Proc. Natl. Acad. Sci. USA* **2020**, *117*, 121.
- [15] S. Laib, R. M. Robertson, D. E. Smith, *Macromolecules* **2006**, *39*, 4115.
- [16] M. Q. Tu, O. Davydovich, B. Mei, P. K. Singh, G. S. Grest, K. S. Schweizer, T. C. O'Connor, C. M. Schroeder, *ACS Polym. Au* **2023**, *3*, 307.
- [17] F. M. Haque, S. M. Grayson, *Nat. Chem.* **2020**, *12*, 433.
- [18] D. Kong, S. Banik, M. J. San Francisco, M. Lee, R. M. Robertson Anderson, C. M. Schroeder, G. B. McKenna, *Macromolecules* **2022**, *55*, 1205.
- [19] B. W. Soh, A. R. Klotz, R. M. Robertson-Anderson, P. S. Doyle, *Phys. Rev. Lett.* **2019**, *123*, 048002.
- [20] J. Smrek, J. Garamella, R. Robertson-Anderson, D. Michieletto, *Sci. Adv.* **2021**, *7*, eabf9260.
- [21] E. Raspaud, D. Lairez, M. Adam, *Macromolecules* **1995**, *28*, 927.
- [22] K.-W. Hsiao, C. Sasmal, J. Ravi Prakash, C. M. Schroeder, *J. Rheol.* **2017**, *61*, 151.
- [23] C. Sasmal, K.-W. Hsiao, C. M. Schroeder, J. Ravi Prakash, *J. Rheol.* **2017**, *61*, 169.
- [24] J. Marfai, R. J. McGorty, R. M. Robertson-Anderson, *Adv. Mater.* **2023**, *35*, 2305824.
- [25] K. R. Peddireddy, M. Lee, Y. Zhou, S. Adalbert, S. Anderson, C. M. Schroeder, R. M. Robertson-Anderson, *Soft Matter* **2020**, *16*, 152.
- [26] T. Ge, S. Panyukov, M. Rubinstein, *Macromolecules* **2016**, *49*, 708.
- [27] T. Sakaue, *Phys. Rev. E* **2012**, *85*, 021806.
- [28] J. Smrek, I. Chubak, C. N. Likos, K. Kremer, *Nat. Commun.* **2020**, *11*, 26.
- [29] J. Wang, T. Ge, *Macromolecules* **2021**, *54*, 7500.
- [30] C. Schneck, J. Smrek, C. N. Likos, A. Zöttl, *Nanoscale* **2024**, *16*, 8880.
- [31] J. D. Halverson, G. S. Grest, A. Y. Grosberg, K. Kremer, *Phys. Rev. Lett.* **2012**, *108*, 038301.
- [32] J. D. Halverson, W. B. Lee, G. S. Grest, A. Y. Grosberg, K. Kremer, *J. Chem. Phys.* **2011**, *134*, 204904.
- [33] G. S. Grest, T. Ge, S. J. Plimpton, M. Rubinstein, T. C. O'Connor, *ACS Polym Au* **2023**, *3*, 209.
- [34] K. R. Peddireddy, R. Clairmont, R. M. Robertson-Anderson, *J. Rheol.* **2023**, *67*, 125.
- [35] M. S. Levy, I. J. Collins, S. S. Yim, J. M. Ward, N. Titchener-Hooker, P. Ayazi Shamlou, P. Dunnill, *Bioprocess Eng.* **1999**, *20*, 7.
- [36] M. M. Diogo, J. A. Queiroz, D. M. F. Prazeres, *J. Chromatogr., A* **2005**, *1069*, 3.
- [37] J. Stadler, R. Lemmens, T. Nyhammar, *J. Gene Med.* **2004**, *6*, S54.
- [38] A. Eon-Duval, G. Burke, *J. Chromatogr., B* **2004**, *804*, 327.
- [39] A. Abdulrahman, A. Ghanem, *Anal. Chim. Acta* **2018**, *1025*, 41.
- [40] M. Hoare, M. S. Levy, D. G. Bracewell, S. D. Doig, S. Kong, N. Titchener-Hooker, P. Dunnill, *Biotechnol. Prog.* **2005**, *21*, 1577.

- [41] M. Gotsmy, F. Strobl, F. Weiß, P. Gruber, B. Kraus, J. Mairhofer, J. Zanghellini, *Microb. Cell Fact.* **2023**, *22*, 242.
- [42] A. E. Carnes, J. A. Williams, (Aldevron LLC), US 7943377B2, **2011**.
- [43] J. Nelson, S. Rodriguez, N. Finlayson, J. Williams, A. Carnes, *Hum. Vacc. Immunother.* **2013**, *9*, 2211.
- [44] A. Tejada-Mansir, R. Montesinos, *Recent Pat. Biotechnol.* **2008**, *2*, 156.
- [45] J. A. Williams, J. Luke, S. Langtry, S. Anderson, C. P. Hodgson, A. E. Carnes, *Biotechnol. Bioeng.* **2009**, *103*, 1129.
- [46] A. Singer, Master Thesis, University of Georgia **2007**.
- [47] A. E. Carnes, J. M. Luke, J. M. Vincent, A. Schukar, S. Anderson, C. P. Hodgson, J. A. Williams, *Biotechnol. Bioeng.* **2011**, *108*, 354.
- [48] D. M. F. Prazeres, T. Schluep, C. Cooney, *J. Chromatogr. A* **1998**, *806*, 31.
- [49] A. E. Carnes, J. A. Williams, in *DNA Vaccines: Methods and Protocols*, (Eds: M. Rinaldi, D. Fioretti, S. Iurescia), Humana Press, NY **2014**.
- [50] J. R. Sayers, D. Evans, J. B. Thomson, *Anal. Biochem.* **1996**, *241*, 186.
- [51] J. Urthaler, C. Ascher, H. Wohrer, R. Necina, *J. Biotechnol.* **2007**, *128*, 132.
- [52] J. L. Wright, M. Jordan, F. M. Wurm, *Cytotechnology* **2001**, *35*, 165.
- [53] H. C. Birnboim, J. Doly, *Nucl. Acids Res.* **1979**, *7*, 1513.
- [54] J. Urthaler, R. Necina, C. Ascher, H. Woehrer, (Boehringer Ingelheim am Rhein (DE)), WO 2004/085643 A1, **2004**.
- [55] N. C. Wan, D. S. McNeilly, C. W. Christopher, (Genzyme Corp), Aus. 706857B2, **1997**.
- [56] H. Hebel, H. Attra, A. Khan, R. Draghia-Akli, *Vaccine* **2006**, *24*, 4607.
- [57] P. Guerrero-Germán, R. Ma. Montesinos-Cisneros, D. M. F. Prazeres, A. Tejada-Mansir, *Biotechnol. Appl. Biochem.* **2011**, *58*, 68.
- [58] A. Padilla-Zamudio, P. Guerrero-Germán, A. Tejada-Mansir, *Bioprocess Biosyst. Eng.* **2015**, *38*, 1091.
- [59] C. Antoniou, Plasmid DNA Clarification, *US Patent 7,700,762 B2*, **2010**.
- [60] L. Zhong, K. Srirangan, J. Scharer, M. Moo-Young, D. Fenner, L. Crossley, C. Howie Honeyman, S.-Y. Suen, C. Perry Chou, *Sep. Purif. Technol.* **2011**, *83*, 121.
- [61] Ion Exchange Chromatography Principles and Methods, GE Healthcare, **2016**.
- [62] T. G. Mason, A. Dhople, D. Wirtz, *Macromolecules* **1998**, *31*, 3600.
- [63] P. Khanal, K. R. Peddireddy, J. Marfai, R. McGorty, R. M. Robertson-Anderson, *J. Rheol.* **2022**, *66*, 699.
- [64] K. R. Peddireddy, M. Lee, Y. Zhou, S. Adalbert, S. Anderson, C. M. Schroeder, R. M. Robertson-Anderson, *Soft Matter* **2019**, *16*, 152.
- [65] K. R. Peddireddy, M. Lee, C. M. Schroeder, R. M. Robertson-Anderson, *Phys. Rev. Res.* **2020**, *2*, 023213.
- [66] H. Isambert, A. C. Maggs, *Macromolecules* **1996**, *29*, 1036.
- [67] A. Rosa, E. Orlandini, L. Tubiana, C. Micheletti, *Macromolecules* **2011**, *44*, 8668.
- [68] P. Neill, N. Crist, R. McGorty, R. Robertson-Anderson, *Soft Matter* **2024**, *20*, 2750.
- [69] D. Michieletto, M. S. Turner, *Proc. Natl. Acad. Sci. USA* **2016**, *113*, 5195.
- [70] D. Michieletto, D. Marenduzzo, E. Orlandini, M. S. Turner, *Polymers* **2017**, *9*, 349.
- [71] D. Michieletto, N. Nahali, A. Rosa, *Phys. Rev. Lett.* **2017**, *119*, 197801.
- [72] Q. Huang, J. Ahn, D. Parisi, T. Chang, O. Hassager, S. Panyukov, M. Rubinstein, D. Vlassopoulos, *Phys. Rev. Lett.* **2019**, *122*, 208001.
- [73] R. Pasquino, T. C. Vasilakopoulos, Y. C. Jeong, H. Lee, S. Rogers, G. Sakellariou, J. Allgaier, A. Takano, A. R. Brás, T. Chang, S. Gooßen, W. Pyckhout-Hintzen, A. Wischniewski, N. Hadjichristidis, D. Richter, M. Rubinstein, D. Vlassopoulos, *ACS Macro Lett.* **2013**, *2*, 874.
- [74] M. Kapnistos, M. Lang, D. Vlassopoulos, W. Pyckhout-Hintzen, D. Richter, D. Cho, T. Chang, M. Rubinstein, *Nat. Mater.* **2008**, *7*, 997.
- [75] C. D. Chapman, K. Lee, D. Henze, D. E. Smith, R. M. Robertson-Anderson, *Macromolecules* **2014**, *47*, 1181.
- [76] M. Rubinstein, R. H. Colby, *Polymer Physics*, Oxford University Press, New York **2003**.
- [77] R. G. Larson, *The Structure and Rheology of Complex Fluids*, Oxford University Press, New York **1999**.
- [78] P.-G. de Gennes, *Scaling Concepts in Polymer Physics*, Cornell University Press, Ithaca, New York **1991**.
- [79] T. G. Mason, A. Dhople, D. Wirtz, *MRS Proc.* **1996**, *463*, 153.